Tribology International 187 (2023) 108768

Contents lists available at ScienceDirect

Tribology International

journal homepage: www.elsevier.com/locate/triboint

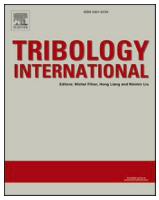

How accurate is the Archard law to predict wear of UHMWPE in hard-on-soft hip implants? A numerical and experimental investigation

Lorenza Mattei *, Francesca Di Puccio

Department of Civil and Industrial Engineering, Largo Lucio Lazzarino 2, Pisa 56126, Italy

ARTICLE INFO

Keywords:
Hip implants
Ceramic-on-plastic
FE wear model
Archard wear law
Model validation
Wear maps

ABSTRACT

Advanced finite element wear models have been recently proposed for hard-on-soft hip implants, but their high computational cost and validation are still open issues. This study aims to develop a fast and accurate wear model for in-silico pre-clinical trials. A finite element model of a ceramic-on-UHMWPE hip implant, based on the Archard wear law, was calibrated and validated using experimental wear maps, as rarely done in the literature. Predicted wear volume and depths deviated from the experimental ones of about 0.2 % and 12–25 %, respectively, comparable to more advanced models including the cross-shearing. Results support the development of relatively simple models requiring limited simulation times, thus making feasible thousands of simulations requested by in-silico trials.

1. Introduction

Wear predictive models of hip implants (HIs) are gaining more and more interest for the pre-clinical assessment of these medical devices since they allow to obtain information on their long-term performance, rapidly and at relatively low cost compared to the time-consuming and expensive in-vitro wear tests. As reviewed in [1,2], many wear models have been proposed in the last decades for hip implants, mainly focused on hard-on-soft (HoS) couplings characterized by liners in UHMWPE, that have a higher wear rate compared to hard-on-hard implants [2]. The wear behavior of UHMWPE is known to be affected by the cross-shearing (CS) [3], which has strongly motivated both experimental and numerical research. Basically, the cross-shearing consists in the local re-alignment of the polymeric chains of UHMWPE in the so called direction of principal molecular orientation depending on the sliding direction, so that the wear resistance, i.e. the wear coefficient k, varies over the contact surfaces and in time. From the first experimental observation of the cross shearing by Wang et al., many different equations have been proposed to quantify the phenomenon with specific wear laws, based on measurements from multidirectional sliding pin-on-disc wear tests [5–8], and also considering the variation of CS with the contact pressure [4]. Such wear laws were implemented in a few finite element (FE) wear models of metal-on-polyethylene HIs [9–11] and compared by the authors using an analytical wear model [12]. Results demonstrated that CS modelling can affect wear predictions, both the wear volume and the wear depth, although, according to most of CS formulations, wear maps obtained by modelling CS are qualitative comparable to that one obtained using a constant wear factor, i.e. the Archard wear law [12]. Unfortunately, the debate on the validation of wear laws for CS modelling is still open: many different laws can be found in the literature, predicting different wear rates, none being fully validated [1,12].

Strictly related to the CS, is the frictional contact modelling, recently investigated by the authors [13]. Although the friction coefficient f is assumed to be constant (more often null) in most wear models of HoS HIs, in the real scenario it varies with the operating conditions and the lubrication regime. In particular, experimental wear tests showed that friction coefficient in HoS couples decreases with the contact pressure [14] and in-vivo measurements by means of instrumented hip implants highlighted friction coefficient variations during a gait cycle [15]. However, results in [13] validate the modelling of frictionless contact when $f < 0.1$, i.e. in most of the scenarios of HoS implants.

An enhanced FE wear model of metal-on- polyethylene HIs has been recently proposed by Liu et al. in [16], where a novel wear law for UHMWPE, including both CS and frictional variation, is formulated based on experimental data from pin-on-disc wear tests [14]. However, it is worth noting that most wear models in the literature are based on the Archard wear law, indeed only 2 out of 26 wear models according to the recent review [1] include the CS and only one a variable friction coefficient ([16]).

* Corresponding author.
E-mail address: lorenza.mattei@unipi.it (L. Mattei).

https://doi.org/10.1016/j.triboint.2023.108768
Received 9 May 2023; Received in revised form 30 June 2023; Accepted 4 July 2023
Available online 5 July 2023

One of the main limits of FE wear models of HIs, is certainly their complexity and the computational cost. On one hand, the CS modelling requires to solve a minimum problem locally, over the whole contact surfaces; on the other hand, long term wear predictions, typically requires the simulation of 2–5 millions of gait cycles, and frequent geometry updates to consider the evolution of the worn contact surfaces. The latter entails the coding of ad-hoc subroutines and thousands of 3D non linear contact analysis, that means very long time simulations. Although numerical strategy such as the acceleration factor [17] and the submodeling technique [18] can help to reduce the computational cost, the model complexity may limit the model applicability in sensitivity analysis to implant design, fundamental in in silico pre-clinical trials, based on thousands of simulations, that are recently gaining more and more interest in the scientific community [19,20]. To note that analytical wear models are very fast compared to FE ones but they cannot predict long term wear, as they do not implement geometry variations due to wear. Another approach that has been pursued in [21] to overcome such limitations is based on machine learning and data-driven modelling. However, a rather huge dataset is necessary to train the model, which can be not so easily available for hip implants as for pin-on-disc tests considered in [21].

A further critical issue is the model validation [1]. Most wear models are based on indirect validation, by comparing FE results with in-vivo and in-vitro wear data collected from very different tribological scenarios. However, the model validation should be direct, i.e. based on the comparison of numerical and experimental of both global and local wear indicators, obtained for the same wear tests, which means same implant type, size and positioning, and same motion and loading conditions. The validation through wear maps is fundamental since the same wear volume can be distributed in a completely different manner on the worn surfaces, thus corresponding to completely different wear maps [12,22]. Nevertheless, only a few models are validated directly [10,16,23–25] and, among these studies, a clear comparison of the numerical and experimental wear maps is proposed only by the most recent ones [16, 25]. The main reason of a so small number of wear models validated directly consists in the difficulty to reconstruct wear maps because of long procedures and the need of expensive laboratory equipment [26]. Rather surprisingly, the wear model proposed in [25] shows wear rate discrepancies compared to experimental results, of the same magnitude order (9–17 %) of [16] (8–25 %) although the former is based on the Archar wear law, whilst the latter on the most advanced wear models.

Moving from these two key points, i.e. the need to reduce model complexity and simulation time, and to validate the model through experimental wear maps, the present paper aims to question whether and how much a relative simple and computationally cheap numerical wear model based on the Archard wear law can predict the real tribological scenario of HoS HIs. The final goal is to develop an accurate fast model to be appliable in in silico pre-clinical trials. To this purpose, experimental and numerical investigations of a ceramic-on-UHMPWE 32 mm hip implant were carried out: a FE model of the in-vitro wear test was developed and validated considering the evolution of the wear maps during the wear test and the applicability and accuracy of the Archard wear law discussed.

2. Methods

2.1. Hip simulator wear test

The tested sample consisted in a 32 mm ceramic-on-plastic HI provided by Permedica S.p.A and characterized by the Jump System® insert in traditional UHMWPE and the head in Biolox Delta®, as shown in Fig. 1(a), with the cup fixed in a metal backing.

The wear test was performed in a single station hip joint simulator, the KUPA E-Sim [26], where the implant was mounted in the anatomical position, with the cup positioned above the head and inclined with respect to it, and maintained in lubricated conditions using calf serum

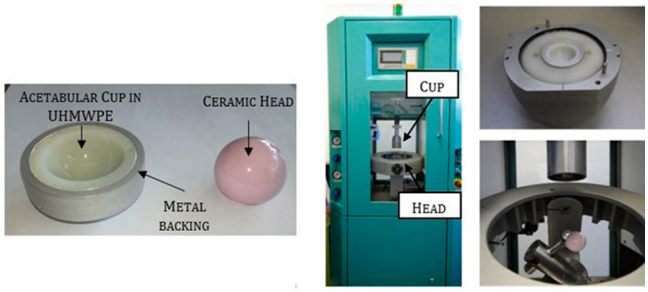

Fig. 1. Sample of ceramic-on-UHMWPE hip implant (a) tested in the KUPA E-Sim hip joint simulator (b) (Edited with permission by Elsevier [26]).

diluted with deionized water and filtered.

The ISO 14242-2 for wear testing of HIs was adopted for test procedure: the gait cycle conditions were simulated for a total of 2 millions of cycles (Mc), with a vertical load combined to 3D relative motion between the head and cup. Wear assessment was performed every 0.5 Mc, i.e. at 0.5, 1, 1.5 and 2 Mc, and both global and local wear indicators were investigated. Gravimetric measurements were performed both on a test sample and a control one (same size of the test sample, loaded but in absence of relative motion), to consider the weight variation caused by lubricant adsorption. Mass variation was converted in worn volume using liner density, so providing volumetric wear data. As far as the local indicators are concerned, wear maps were obtained using a focus variation microscope for non-contact surface characterization, the InfiniteFocus G5 by Alicona®. The replica method was adopted, combined to the procedure for point cloud registration and wear map computation, as described in [26]. Consequently, the evolution of the wear map could be investigated.

2.2. FE wear model

A FE model reproducing the wear test described in Section 2.1 was developed using Ansys Workbench®.

The main model parameters are summarized Table 1.

2.2.1. Geometry, materials and mesh

The hip implant was modeled as a spherical joint with exactly the same geometry of the test sample. The head and cup diameters were 31.956 mm and 32.490 mm, respectively, thus resulting a radial clearance of 267 μm. The cup thickness was of 5 mm. The anatomical position of the implant was reproduced by an inclination angle of the cup $\beta = 60°$ between the cup axis and the horizontal plane. The geometry is shown in Fig. 2(a, b).

Table 1
Summary of the geometrical and material properties, and of contact and wear parameters of the FE model. Legend: k_{nc} non-calibrated wear coefficient; k_c calibrated wear coefficient for the running-in (ri) and the steady state phases (ss); N_{ug} number of wear cycles between two consecutive geometry updates for the running-in (ri) and the steady state phases (ss).

Geometry	Head diameter (mm)	31.956
	Cup diameter (mm)	32.490
	Radial clearance (mm)	0.267
	Cup thickness (mm)	5
	β (°)	60
Materials	UHMWPE Young's modulus (MPa)	500
	UHMWPE Poisson's ratio	0.4
Contact and wear	k_{nc} (mm^2/N)	$1.066\ 10^{-9}$
	k_c^{ri} (mm^2/N)	$2.751\ 10^{-9}$
	k_c^{ss} (mm^2/N)	$8.839\ 10^{-10}$
	N_{ug}^{ri} (Mc)	0.056
	N_{ug}^{ss} (Mc)	0.25

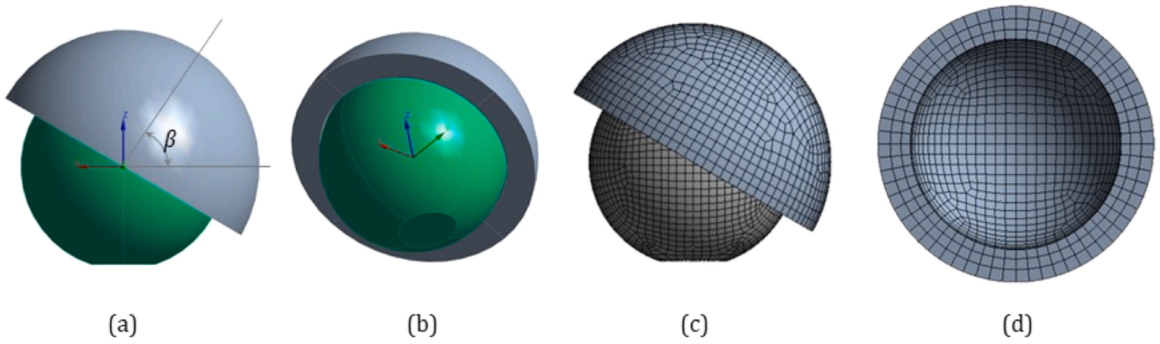

Fig. 2. Model geometry (a, b) and mesh (c) with a detailed view on the mesh of the cup contact surface (d).

The flexible-on-flexible contact between the head and cup was simplified as a flexible-on-rigid one, being the ceramic head extremely stiffer than the plastic cup, in agreement with the literature [1]. This is feasible also considering that the wear is unilateral, i.e. affects only the cup, whilst no wear occurs at the head, as also confirmed by experimental inspection of the tested head sample. The traditional UHMWPE of the liner was modeled as a linear elastic, isotropic and homogeneous material with a Young's modulus of 500 MPa and a Poisson's ratio of 0.4. Although UHMWPE exhibits viscoelastic properties, linear elasticity was assumed to reduce both model complexity and computational time, aim of the present work. In the literature, only few studies assume UHMWPE viscoelastic material (just one [23] out of 26 studies considered in the recent review [1]).

The model mesh, shown in Fig. 2(c, d), was selected after an accurate sensitivity analysis, based on the contact pressure convergence, as a compromise between the model accuracy and the computational cost. The mesh was obtained using geometrical divisions of the body surfaces (lines in light gray visible in Fig. 2(a, b), and combing multizone, edge sizing and face sizing methods. The mesh was refined on the contact surfaces, resulting element size ranging from 1.25 mm at the contact surfaces to 1.5 mm far from contact (i.e. at the cup external surface). The head mesh neither affected wear results nor the computational cost. Hexahedral elements of second order, i.e. SOLID186 were used to mesh the cup, whilst the contact surfaces of cup and head were meshed with CONTA174 and TARGE170 elements, respectively.

2.2.2. Contact modeling

The interaction between the head and cup surfaces was modelled as a frictionless dry contact. This frictionless hypothesis is supported by the recent investigations of the authors on the effect of friction on wear parameters, that resulted negligible for friction coefficient lower than 0.1, as in case of ceramic-on-plastic HIs, [13]. Also the dry contact condition is a well-accepted hypothesis in the literature that allows to develop a relative simple model, not computationally expensive, aim of the present work. Advanced wear model including also mixed-lubrication effects have been recently proposed for hip implants, such as in [27]. Unfortunately these models are very complex, computationally expensive and typically applied to the simulation of only one gait cycle [27].

However, as far as wear is concerned, it is intended that the effects of roughness and lubricant are included in the experimental estimation of the wear coefficient k (see the following section).

The cup and the head were set as contact and target surfaces, respectively. The contact settings were the following: asymmetric contact (since only the cup gets worn), Augmented Lagrange formulation, nodal-normal to target detection method, penetration tolerance and normal stiffness program controlled and update stiffness at each iteration. It is worth noting that this contact settings are fundamental for the model convergence and accurate results. The contact surfaces interaction is affected by the wear process that continuously modifies the surface geometry, as detailed in Section 2.2.3.3.

2.2.3. Wear modeling

2.2.3.1. Wear law. The main wear mechanisms of the plastic cup were considered as the abrasive and adhesive ones, described by the well-known Archard wear equation that establishes a linear relation between the wear volume V and the product of the contact force normal L_N to the contact and the sliding distance s according to:

$$V = k \quad L_N \quad s \tag{1}$$

Where k is the wear coefficient. In 3D contact problems, with time varying contact force and contact conditions variable on the contact surface, the Archard wear law is re-written in a local instantaneous form for a contact point Q at the time t, as:

$$\dot{h}(Q,t) = k \quad p(Q,t) \quad v_s(Q,t) \tag{2}$$

Where $\dot{h}$ is the linear wear rate, p is the contact pressure and v_s is the sliding velocity. As discussed in the introduction, more advanced wear laws/wear coefficient expressions have been proposed in the literature to model wear of UHMWPE and its CS. It is worth noting that the wear coefficient is a complex parameter dependent on the tribological scenario, and thus varying in space and time, both during a single wear cycle and the whole wear process. In particular, it has been described as a function of the CS [10]. However, being the objective of the present study to develop a simple, fast and accurate model through the assessment of the goodness/limits of the Archard wear law, only the latter was considered, assuming a constant wear coefficient.

Thus Eq.(2) was implemented in the FE model through the APDL command TB, WEAR inserted in the contact environment, and properly set. Activating the option ARCH, the generalized form of the Archard wear law is implemented:

$$\dot{h}(Q,t) = \frac{K}{H} \quad p^m(Q,t) \quad v_s^n(Q,t) \tag{2}$$

Where H is the material hardness. The equation of interest (2) was obtained by setting $k = K/H$ and $m = n = 1$ using the *TB, DATA* command. The time interval of the wear process was then specified through the *TB, FIELD* command. To note that the *TB, WEAR* command automatically moves the contact nodes normal to the contact surfaces considering the sliding distance traveled by Q in the time interval Δt between two consecutive contact analyses, as it follows:

$$\Delta h(Q,t) = k \quad p(Q,t) \quad v_s(Q,t) \quad \Delta t \tag{3}$$

2.2.3.2. Wear coefficient estimation. The estimation of the wear coefficient, that implicates the FE model calibration, was based on the comparison of the numerical and experimental wear volumes, V_{num} and V_{exp}, respectively, obtained simulating the same test conditions. Once predicted the V_{num} using a non calibrated wear coefficient k_{nc}, the calibrated wear coefficient, k_c, was obtained as:

$$k_c = \frac{V_{exp}}{V_{num}} k_{nc} \quad (4)$$

Since the experimental results demonstrated the existence of an initial running-in phase (RI), covering the first 0.5 Mc, followed by a steady state phase (SS), from 0.5 to 2 Mc [26], two distinct and constant wear coefficients were estimated for the two phases.

As a first step, the simulation was run only for the RI, using a value of 1.066 10^{-9} mm^2/N for k_{nc}, taken from the literature [28,29]. According to Eq.(4), the calibrated wear coefficient of the RI, k_c^{ri}, resulted 2.751 10^{-9} mm^2/N. This value was then used as k_{nc} for the SS, and thus to run its simulation. Again using Eq.(4), a calibrated wear coefficient for the steady state phase, k_c^{ss}, equal to 8.839 10^{-10} mm^2/N, was computed. The summary of the adopted wear coefficient is given in Table 1.

It is worth noting, the model calibration was based on a trial and error procedure, parallel to the estimation of the frequency of the geometry update, explained in the next paragraph. Actually, only two trials were sufficient for accurate results. For both k_c^{ri} and k_c^{ss}, in the first trial, three geometry updates were performed during the simulation of each phase. In the second trial, the frequency of the geometry update was set to the convergence value evaluated though a proper sensitivity analysis.

2.2.3.3. Frequency of geometry update. Since the wear in a gait cycle is very low (of about of 10^{-7} mm), and millions of wear cycles should be simulated, a double strategy was used for the geometry update:

i) within a single wear cycle, the wear coefficient was amplified by a factor 10, thus reducing the total number of cycles by 1/10 (i.e. from 2 Mc to 0.2 Mc).
ii) the wear produced in a single cycle was then further amplified to extrapolate the wear increment after N_{ug} *cycles, number of wear cycles between two consecutive geometrical updates* [16,23,25]. The estimation of N_{ug} *required a sensitivity analysis since a too low value of* N_{ug} *causes useless long simulation times, whilst a too high value of* N_{ug} *causes the prediction of unreliable worn profiles, with typical strong discontinuities of the local curvature radii at the edges of the worn area associated to unreliable peaks of contact pressure.*

In this study, two distinct values of N_{ug} were evaluated for the running-in and the steady state phase by varying N_{ug} in the range 0.033–0.25 Mc, that corresponds to the repetition of 2–15 UPGEOM procedures in 0.5 Mc. Such sensitivity analysis provided N_{ug}^{ri} and N_{ug}^{ss} for the RI and SS, respectively of 0.056 Mc and 0.25 Mc (see Table 1). Indeed, during the running-in the wear rate is higher compared to the steady state and consequently a more frequent geometrical update was necessary. It is worth noting that the use of distinct values of N_{ug}^{ri} and N_{ug}^{ss} allowed to greatly reduce the computational time.

2.2.4. Loading and motion conditions

The loading and the kinematic conditions were prescribed according to ISO 14242 to simulate a gait cycle. The external surface of the cup was built-in whilst both the load and the motions were applied to the head, as shown in Fig. 3(a). The vertical load was applied as a remote force at the center of head, using the cut surface at the head bottom. The head motion was prescribed through a general joint with 6 DoFs that enabled to drive both translations and rotations. The translations were left free as controlled by the load, whilst the rotations were set to simulate the sequence of Flexion-Extension (FE), Adduction-Abduction (AA), Inward-Outward rotation (IO), i.e. FE→AA→IO, as rotations sequence x→y→z around local axes. The load and rotations curves are reported in Fig. 3(b) and (c) respectively.

A sensitivity analysis was performed to evaluate the number of simulation steps within each gait cycle, resulting in 50 steps, that means a contact analysis every 0.02 s.

3. Results and discussions

3.1. FE model calibration

As explained in Section 2.2.3.2, the FE model calibration is based on the estimation of the wear coefficients, exploiting wear volumes from in-vitro tests. The experimental curves of the wear volume V shown in Fig. 4, revealed two distinct phases of the wear process, the running-in occurring before 0.5 Mc, and the following steady state phase [26]. Consequently, two distinct wear coefficients were estimated for the two phases, k_c^{ri} resulting higher than k_c^{ss} given the higher wear rate of the RI compared to the SS (Table 1). Using such values of k, the FE model was able to predict the experimental wear volumes at 0.5 Mc and 2 Mc, with a deviation of about 0.2 %. Moreover, the model well predicted also the linear trend of the experimental V, in agreement both with the Archard

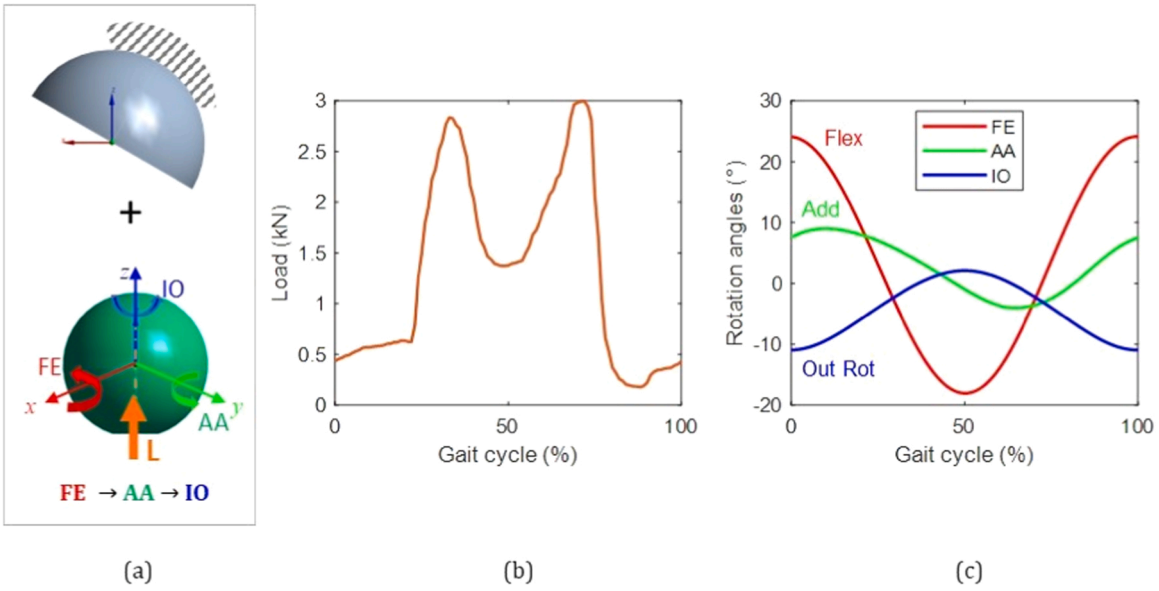

Fig. 3. Loading and motion conditions of a gait cycle: the cup was fixed whilst the load and the motion were applied both to the head (a). Load (b) and rotations (c) curves followed ISO 14242. Legend: FE: Flexion-Extension; AA: Adduction-Abduction; IO: Inward-Outward rotation.

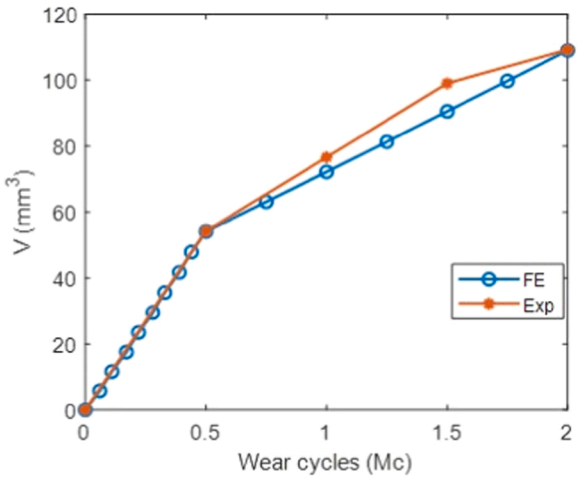

Fig. 4. Comparison of the FE and the experimental trends of the wear volume V during the wear test.

equation and literature studies (e.g. [5,18]).

To note that a calibrated model is not validated. Indeed, although the FE model was able to predict experimental *V*, this does not imply that the wear distribution over the contact surfaces is the same, i.e. equal FE and experimental wear maps. The model validation will be discussed in Section 3.3.

3.2. FE model predictions

3.2.1. Contact pressure

Compared to experimental investigation, the FE model was able to provide information on contact actions exchanged between the cup and the head surfaces, which, being the contact frictionless, had only a component normal to the surface, i.e. the contact pressure. As explained in Section 2.2.3, the contact pressure is variable with the space and time, $p(Q,t)$. Consider first the evolution of the contact pressure at a "special" cup point aligned with the loading direction, i.e. the nominal contact point: it is the point where the maximum contact pressure p_{max} was observed, both during a single gait cycle and overall the whole the wear process [13]. The temporal evolution of p_{max} is shown in Fig. 5(a): its trend during a single gait cycle recalls the trend of the loading curve with two peaks (Fig. 3(b)), during the whole process, i.e. independently from the considered number of wear cycle n_{wc}. However, on the other hand, comparing p_{max} at different n_{wc}, it resulted that the contact pressure changed significantly from a quantitative point view: as the surfaces worn out, the wear caused a more conformal contact and thus a substantial and fast decrease of the contact pressure. That is well captured by the evolution of the value of p_{max} taken at the second load peak (the highest), p_{max2}, plotted in Fig. 5(b). Results demonstrated that p_{max2} changed quickly and non linearly during the running-in: after the first geometrical change at 0.06 Mc, it was reduced of about 18 % and was more than halved (54 % reduction) at 0.5 Mc. However, during the steady state phase, p_{max2} decreased more slowly, almost linearly with n_{wc}, reducing only of a further 8 % at the end of the simulation. The percentage variation rate of p_{max2} was of about -110 %/Mc and -6 %/Mc for the RI and SS, respectively.

A more complete description of the contact conditions at different n_{wc} is provided by the contact pressure maps reported in Fig. 6 for the cup and at the second load peak. In Fig. 6(a), the maps are plotted each one on its full scale, allowing to catch at the best the contact pressure variation over the contact surface, while in (b) they are plotted on the same scale to facilitate their comparison. It can be observed that, first of all, the contact area remained always located in the medial side of the cup ($x > 0$), in agreement with the cup positioning and the fixed loading direction. In new conditions (0 Mc), the contact pressure was perfectly symmetric with respect to the loading direction, whilst, as the wear progressed, it lost such a symmetry and the area affected by the highest contact pressure values (the red regions) became slightly oval, stretched in the medial-lateral direction. That was more evident after 0.22 Mc. Also the evolution of the contact pressure maps, in agreement with the trend of p_{max} and p_{max2}, demonstrated that the wear damage caused a more conformal contact, with wider contact regions and lower values of contact pressures, as clearly showed in Fig. 6(b). That representation of the contact pressure allows to highlight the enlargement of the contact area, and, mostly, the more uniform distribution of contact pressure with wear evolution. Note that the red area almost disappeared at 0.11 Mc.

3.2.2. Wear prediction/assessment

The FE wear model was developed to predict the evolution of surface damage during the wear process, providing both global (volume, area) and local (linear depth) indicators on the material loss caused by the wear. Remarkably, in this case, a comparison with experimental results was possible and allowed both the model calibration and validation, as described in the following section.

The trend of worn volume *V* during the wear process is plotted in Fig. 4(a) and is in good agreement with experimental results: according to the model, it increases bilinearly with the wear cycles and its rate of change depends on the wear coefficient and thus is higher during the RI

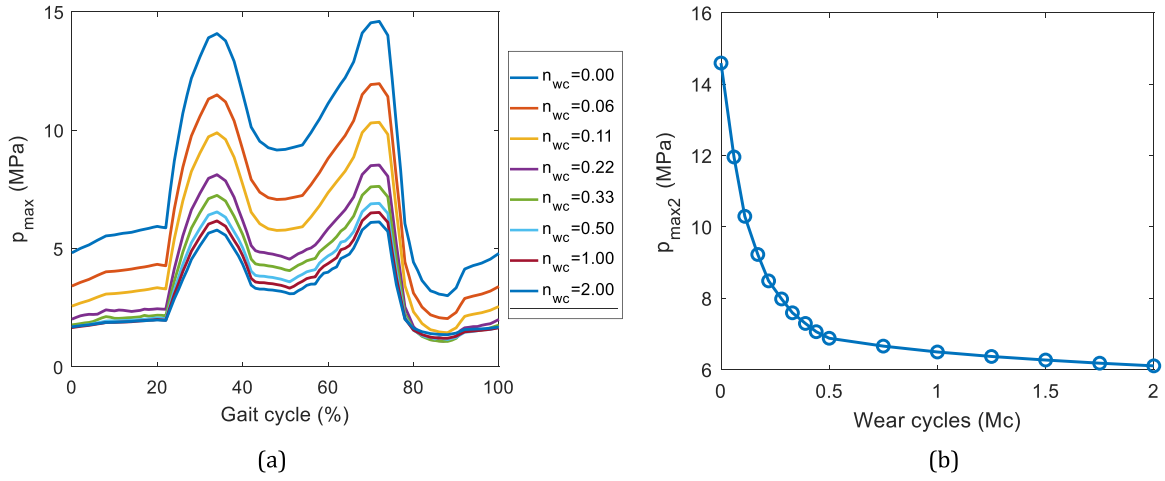

Fig. 5. Evolution of the trends of the maximum contact pressure p_{max} during a gait cycle, at different numbers of wear cycles, n_{wc} (in Mc) (a). Evolution of the maximum contact pressure evaluated at the second load peak p_{max2}, during the wear process (b).

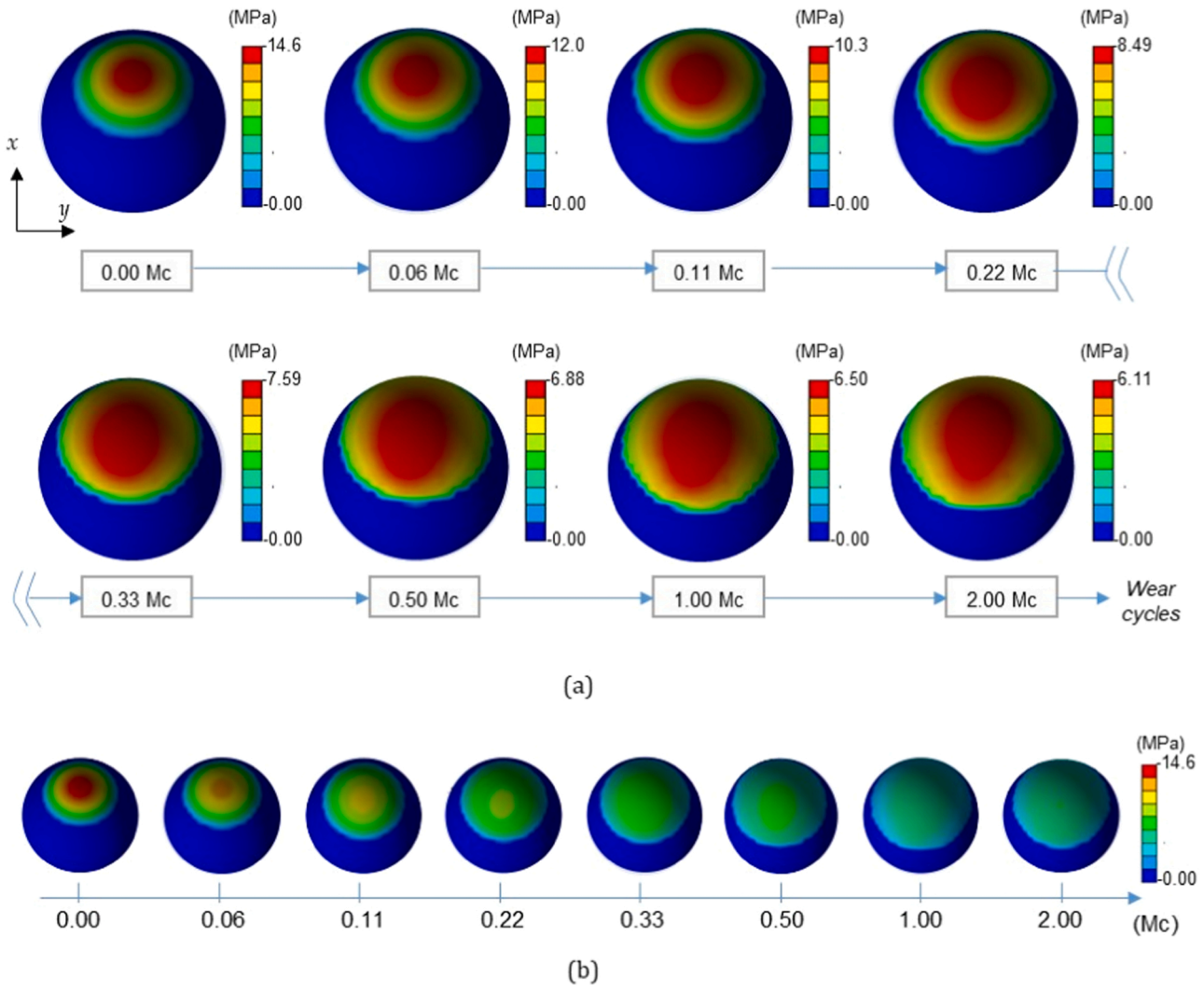

Fig. 6. Evolution of the numerical contact pressure maps during the wear process. The maps at the second load peaks, at different number of wear cycles, are plotted each one in its full scale (a) and compared on the same scale (b).

and lower in the SS. The worm volume at the end of the running was predicted to be 54.1 mm^3, whilst the final one, at 2 Mc, 109 mm^3, thus resulting in volume rates of 108.1 and 36.6 mm^3/Mc respectively for the two phases with a ratio of about 3:1 (as for k values).

As a local indicator, the maximum wear depth h_{max} over the worn area was first considered. As already observed, due to the loading and conditions, the nominal contact point between the surfaces remained fixed on the cup. Such point experienced both p_{max} and h_{max}. As depicted in Fig. 7, in agreement with the trend of V, h_{max} increased faster during the RI compared to the SS. However, differently from the V trend, the increase of h_{max} was not linear during the RI and became linear only in the steady state phase. During the running-in, the rate of h_{max} decreased with wear cycles because of the more conformal contact. Quantitatively, h_{max} was 0.17 mm at the end of the running-in, and increased up to 0.27 mm at the end of the wear simulation. The wear rate was about 0.33 mm/Mc and 0.07 mm/Mc during the RI and the SS, respectively.

A more complete description of the surface damage was provided by the wear maps captured at different n_{wc} and reported both each one on its full scale and on the same scale (Fig. 8(a) and (b), respectively). Throughout the wear process, the worn region remained located in the same cup region, in the medial side, i.e. in correspondence of the contact area, and it was symmetric with respect to the loading line. The slight asymmetry of the contact pressure maps observed at the second load peak (Fig. 6) during the steady state did not affect the symmetry of the

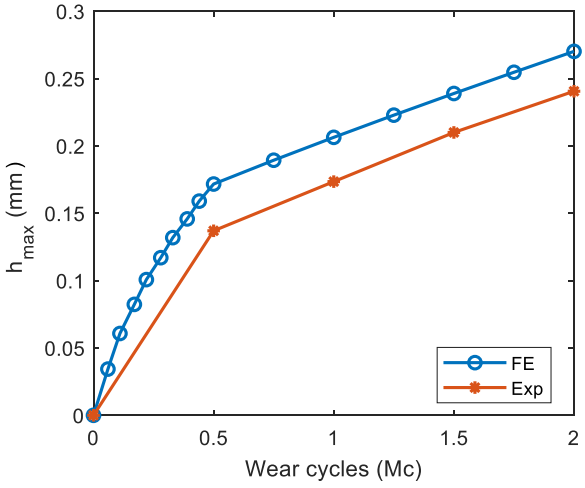

Fig. 7. Comparison of the FE and the experimental trends of the maximum wear depth h_{max}, during the wear test.

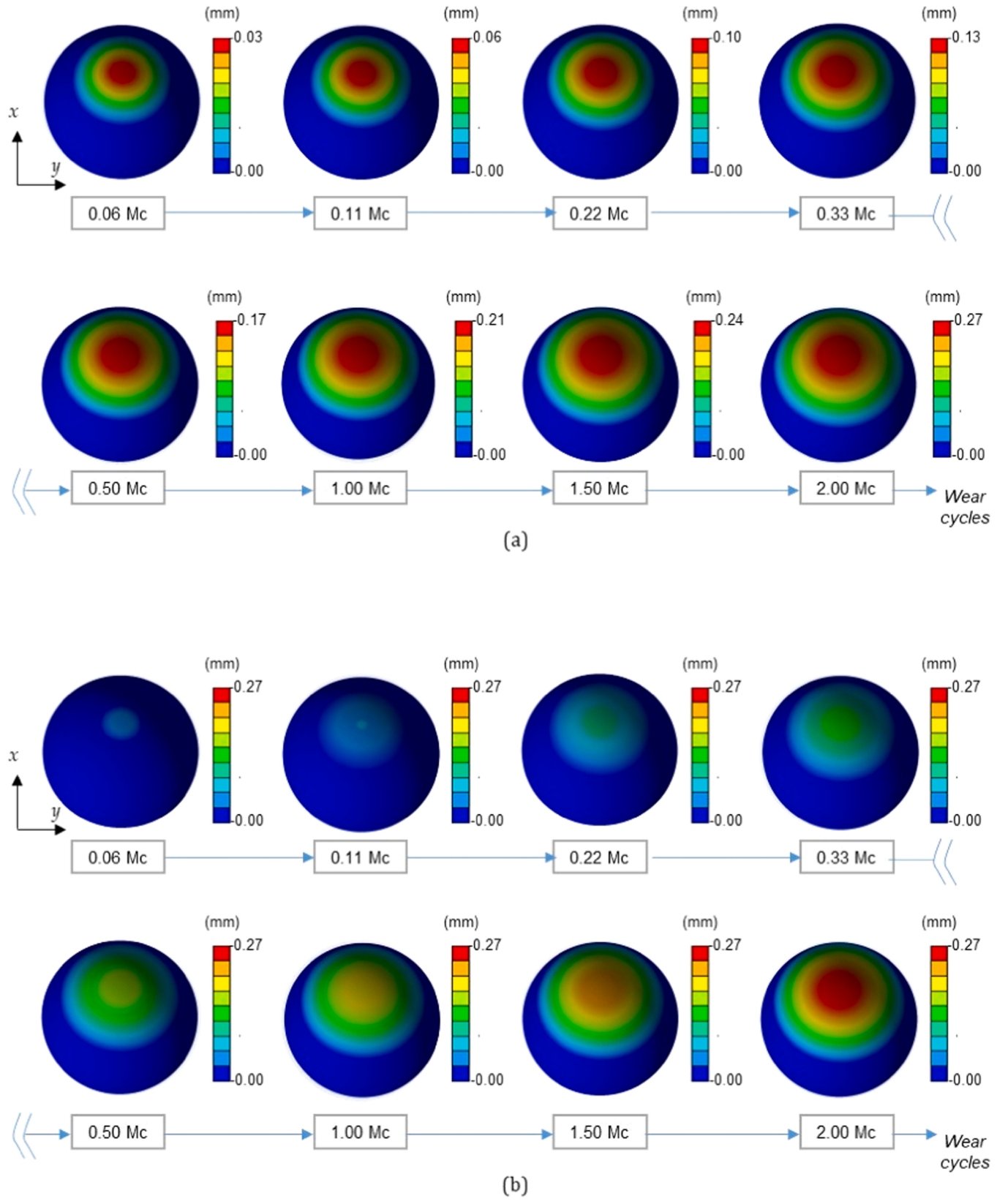

Fig. 8. Evolution of the FE wear maps shown each one on its full scale (a) and compared using the same scale (b).

wear maps. The main reason was that the wear maps reflect, in a cumulative fashion, what happens in the wear process until the considered n_{wc}, whilst the contact pressure map are just an instantaneous picture of the contact conditions. Additionally, consider that worn area depended both on the contact pressure and the sliding distance. For the same reasons, the contact areas shown in Fig. 6, appeared wider than the correspondent worn area, at the same n_{wc}.

The evolution of the wear damage was well captured by the wear

maps reported on the same scale (Fig. 8(b)): although qualitatively the wear maps were very similar and symmetric with respect to the loading line, the worn area increased significantly during the wear tests, reaching the cup medial edge.

As a further global wear indicator, the worn area A_w was considered. The trend of A_w, shown in Fig. 9, was similar to that one of h_{max}: non-linear and more rapid during the RI and linear during the SS. Moreover, during the running-in the increase of A_w slowed down because of the increasing contact conformity. Quantitatively, A_w increased up to 613 mm^2 at 0.5 Mc, and up to 783 mm^2 at 2 Mc. The increase rate of A_w was 1030 mm^2/Mc and 115 mm^2/Mc for the RI and the SS, respectively.

3.3. FE model validation and accuracy of the Archard wear law

The model validation was based on the comparison of the FE and experimental wear maps at the same n_{wc}, i.e. 0.5, 1, 1.5 and 2 Mc, portrayed in Fig. 10. To ease the comparison, the wear maps are plotted on their own full scale were considered and the color levels of the FE wear maps were adapted to the experimental ones. It can be noted that, adopting the new color scale, the red area appears wider. At a first glance, qualitatively, the FE and experimental wear maps were very similar: same location at the cup medial side, comparable extension of the worn areas and comparable areas with the same color. Moreover, in both the FE and experimental wear maps, as the wear advanced, the worn region widened and the mostly worn area moved towards the cup medial side. Of course, also some differences can be noted: FE wear maps were almost perfectly symmetric, whilst the experimental ones were slightly asymmetric mainly because of the deposit of a wear debris (green area in the wear map at 2 Mc, [26]), that is proper of the real wear mechanisms and unpredictable by the Archard wear law.

The quantitative comparison of the wear maps can be made easier considering the value of the maximum wear depth, as done in Fig. 7. As far as the curve of h_{max} is concerned, both the FE and the experimental one reflected the sequence of the RI and SS phases and they are both linear in the SS phase maintaining the gap observed at the end of the RI. Unfortunately, the first experimental wear observation was done at 0.5 Mc, thus the validation of the initial non linear trend of h_{max} was not possible. Additionally, such information on the trend of h_{max} could not be obtained from the literature, since, to the best of authors knowledge, wear data before 0.5 Mc were not available from other studies.

Fig. 7 and Fig. 10 show that the FE model overestimated the experimental h_{max} of nearly 0.03 mm from the RI to the end of the simulation, resulting in a percentage difference of 25 % and 12 % at 0.5 Mc and 2 Mc, respectively. To note that the difference between FE and experimental values of h_{max} occurred in the RI, keeping a constant value in the following SS. Such a quantitative deviation might be imputed to the model itself, e.g. creep that was not considered in the present model [16,30] and the CS was neglected, but also to uncertainties in the experimental maps. However, the model recently presented in [16], based on the most advanced wear law for the UHMWPE and also modeling the creep, reported deviations between FE and experimental wear rates absolutely comparable to the ones of the present study, in the range 8–25 %.

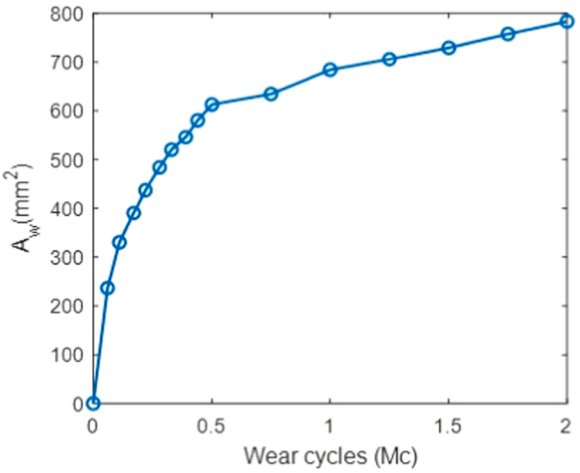

Fig. 9. Evolution of the numerical worn area A_w during the wear process.

4. Conclusions

The present study combines numerical and experimental wear investigations on a ceramic-on-UHMWPE hip implant with the aim to assess the reliability of the Archard law in wear predictive simulations, also when wear is affected by the cross-shearing effect as in UHMWPE. The model was calibrated using experimental wear volumes, distinguishing between a running-in and a steady state phase, and was validated using wear maps, as rarely done in the literature.

The simulation of the running-in, occurring approximately in the first 0.5 Mc, was more critical since the surface geometry changed quickly becoming more conformal, and a high number of geometrical updates were required for accurate results. In this phase, the contact pressure decreased almost exponentially, V increased linearly and h_{max} and A_w non linearly. The full validation of such trends would require more frequent wear measurements during running-in, that will be considered in future studies.

During the steady state phase, the surface geometry varied more slowly, and the numerical trend of both contact and wear parameters was linear. This aspect is interesting, as it suggests that wear at long term could be easily predicted by a linear extrapolation. This aspect will be investigated in future considering longer wear tests/simulations.

In conclusion, the small deviations between numerical and experimental V and h_{max}, as well as the similarity of the correspondent wear maps, fully support the model validation and foster the use of relatively "simple" wear models based on the Archard wear law. That enables to reduce the model computational costs, especially when other aspects have to be include in the model, e.g. a combination of daily motor tasks [31,32] or a mixed lubrication regime [32,33]. These issues are gaining interest in the perspective of in-silico clinical trials [19] of hip implants, requiring a huge number of wear simulations for a wide patient virtual cohort. Future investigations will include an evaluation of model uncertainties, from elements features and mesh definition to geometry, material parameters, and so on in order to assess the credibility of model application in in-silico trials.

Author agreement statement

We the undersigned declare that this manuscript is original, has not been published before and is not currently being considered for publication elsewhere. We confirm that the manuscript has been read and approved by all named authors and that there are no other persons who satisfied the criteria for authorship but are not listed. We further confirm that the order of authors listed in the manuscript has been approved by all of us. We understand that the Corresponding Author is the sole contact for the Editorial process. He/she is responsible for communicating with the other authors about progress, submissions of revisions and final approval of proofs.

Funding

This study was supported by the PRA 2022_25 Grant of the University of Pisa.

Declaration of Competing Interest

All authors have participated in (a) conception and design, or analysis and interpretation of the data; (b) drafting the article or revising it

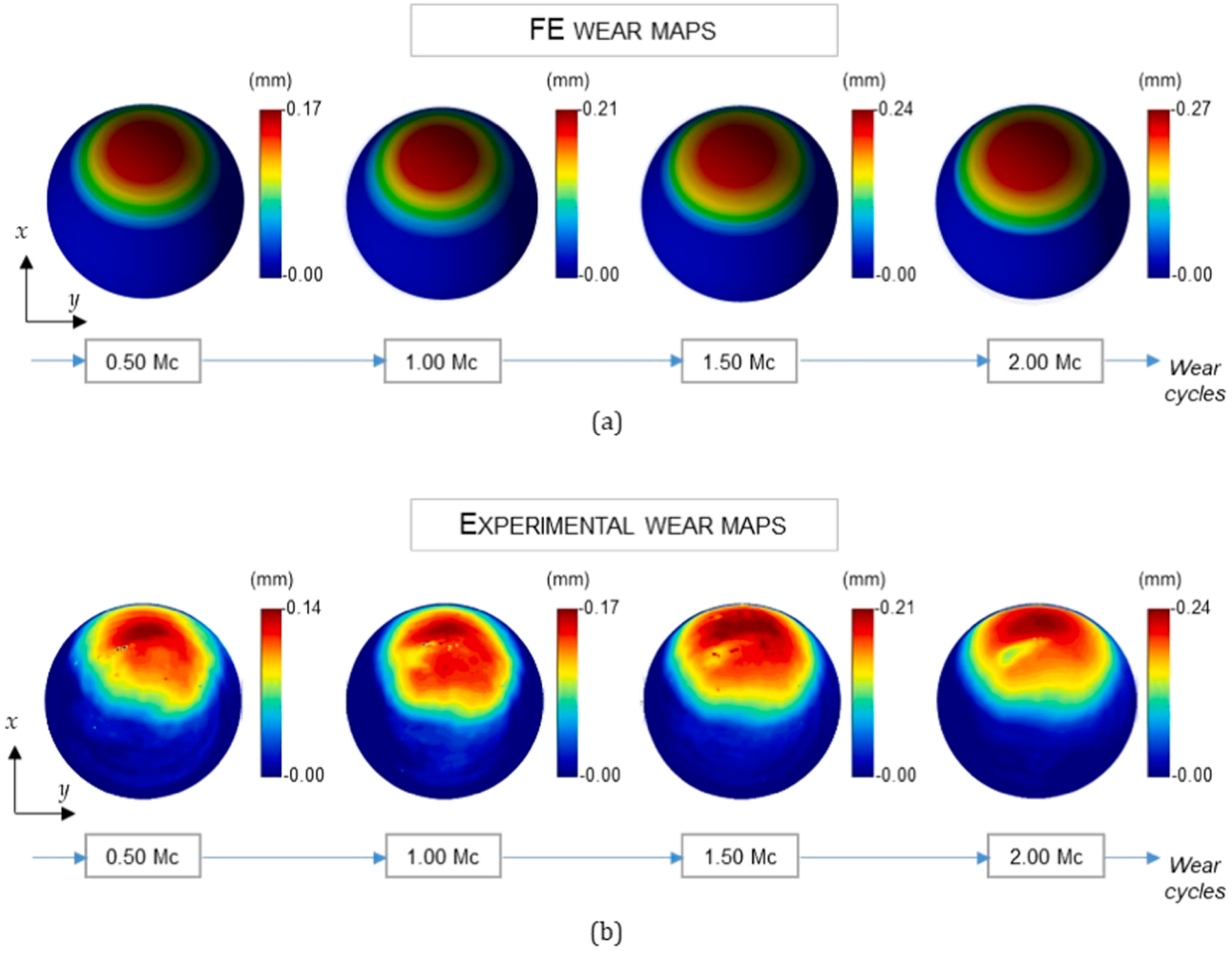

Fig. 10. Comparison of the evolution of the wear maps obtained numerically (a) and experimentally (Edited with permission from Elsevier [26]) (b).

critically for important intellectual content; and (c) approval of the final version. This manuscript has not been submitted to, nor is under review at, another journal or other publishing venue. The authors have no affiliation with any organization with a direct or indirect financial interest in the subject matter discussed in the manuscript.

Data availability

No data was used for the research described in the article.

Acknowledgements

The authors acknowledge Ph.D. Eng. Mattia Moda for his contribution in FE simulations.

References

[1] Wang L, Isaac G, Wilcox R, Jones A, Thompson J. Finite element analysis of polyethylene wear in total hip replacement: a literature review. Proc Inst Mech Eng H 2019;233:1067–88. https://doi.org/10.1177/0954411919872630.
[2] Mattei L, Di Puccio F, Piccigallo B, Ciulli E. Lubrication and wear modelling of artificial hip joints: a review. Tribol Int 2011;44:532–49. https://doi.org/10.1016/j.triboint.2010.06.010.
[3] Wang A. A unified theory of wear for ultra-high molecular weight polyethylene in multi-directional sliding. Wear 2001;248:38–47. https://doi.org/10.1016/S0043-1648(00)00522-6.
[4] Wang A, Essner A, Klein R. Effect of contact stress on friction and wear of ultra-high molecular weight polyethylene in total hip replacement. Proc Inst Mech Eng H 2001;215:133–9. https://doi.org/10.1243/0954411011533698.
[5] Kang L, Galvin AL, Brown TD, Jin Z, Fisher J. Quantification of the effect of cross-shear on the wear of conventional and highly cross-linked UHMWPE. J Biomech 2008;41:340–6. https://doi.org/10.1016/j.jbiomech.2007.09.005.
[6] Dressler MR, Strickland MA, Taylor M, Render TD, Ernsberger CN. Predicting wear of UHMWPE: decreasing wear rate following a change in direction. Wear 2011;271:2879–83. https://doi.org/10.1016/j.wear.2011.06.006.
[7] Strickland MA, Dressler MR, Taylor M. Predicting implant UHMWPE wear in-silico: a robust, adaptable computational–numerical framework for future theoretical models. Wear 2012;274–275:100–8. https://doi.org/10.1016/j.wear.2011.08.020.
[8] O'Brien ST, Bohm ER, Petrak MJ, Wyss UP, Brandt J-M. An energy dissipation and cross shear time dependent computational wear model for the analysis of polyethylene wear in total knee replacements. J Biomech 2014;47:1127–33. https://doi.org/10.1016/j.jbiomech.2013.12.017.
[9] Liu F, Galvin A, Jin Z, Fisher J. A new formulation for the prediction of polyethylene wear in artificial hip joints. Proc Inst Mech Eng H 2011;225:16–24. https://doi.org/10.1243/09544119JEIM819.
[10] Kang L, Galvin AL, Brown TD, Fisher J, Jin Z-M. Wear simulation of ultra-high molecular weight polyethylene hip implants by incorporating the effects of cross-shear and contact pressure. Proc Inst Mech Eng H 2008;222:1049–64. https://doi.org/10.1243/09544119JEIM431.
[11] Kang L, Galvin AL, Fisher J, Jin Z. Enhanced computational prediction of polyethylene wear in hip joints by incorporating cross-shear and contact pressure in additional to load and sliding distance: effect of head diameter. J Biomech 2009;42:912–8. https://doi.org/10.1016/j.jbiomech.2009.01.005.
[12] Mattei L, Di Puccio F, Ciulli E. A comparative study of wear laws for soft-on-hard hip implants using a mathematical wear model. Tribol Int 2013;63:66–77. https://doi.org/10.1016/j.triboint.2012.03.002.
[13] Mattei L, Di Puccio F. Frictionless vs. frictional contact in numerical wear predictions of conformal and non-conformal sliding couplings, 70(4). Tribol Lett 2022;115. https://doi.org/10.1007/s11249-022-01657-5.
[14] Saikko V. Effect of contact area on the wear and friction of UHMWPE in circular translation pin-on-disk tests. J Tribology 2017;139:061606. https://doi.org/10.1115/1.4036448.

[15] Damm P, Bender A, Duda G, Bergmann G. In vivo measured joint friction in hip implants during walking after a short rest. PLoS One 2017;12:e0174788. https://doi.org/10.1371/journal.pone.0174788.
[16] Liu F, He Y, Gao Z, Jiao D. Enhanced computational modelling of UHMWPE wear in total hip joint replacements: the role of frictional work and contact pressure. Wear 2021;482–483:203985. https://doi.org/10.1016/j.wear.2021.203985.
[17] Mattei L, Di Puccio F. Influence of the wear partition factor on wear evolution modelling of sliding surfaces. Int J Mech Sci 2015;99:72–88. https://doi.org/10.1016/j.ijmecsci.2015.03.022.
[18] Curreli C, Di Puccio F, Mattei L. Application of the finite element submodeling technique in a single point contact and wear problem. Int J Numer Methods Eng 2018;116:708–22. https://doi.org/10.1002/nme.5940.
[19] Pappalardo F, Russo G, Tshinanu FM, Viceconti M. In silico clinical trials: concepts and early adoptions. Brief Bioinform 2019;20:1699–708. https://doi.org/10.1093/bib/bby043.
[20] Bodner J., Kaul V. A framework for in silico clinical trials for medical devices using concepts from model verification, validation, and uncertainty quantification (VVUQ), 2021. Available from: https://doi.org/10.1115/VVS2021–65094.
[21] Borjali A, Monson K, Raeymaekers B. Predicting the polyethylene wear rate in pin-on-disc experiments in the context of prosthetic hip implants: Deriving a data-driven model using machine learning methods. Tribol Int 2019;133:101–10. https://doi.org/10.1016/j.triboint.2019.01.014.
[22] Mattei L, Di Puccio F, Joyce TJ, Ciulli E. Numerical and experimental investigations for the evaluation of the wear coefficient of reverse total shoulder prostheses. J Mech Behav Biomed Mater 2016;55:53–66. https://doi.org/10.1016/j.jmbbm.2015.10.007.
[23] Matsoukas G, Willing R, Kim IY. Total hip wear assessment: a comparison between computational and in vitro wear assessment techniques using ISO 14242 loading and kinematics. J Biomech Eng 2009;131:041011. https://doi.org/10.1115/1.3049477.
[24] Maxian TA, Brown TD, Pedersen DR, Callaghan JJ. A sliding-distance-coupled finite element formulation for polyethylene wear in total hip arthroplasty. J Biomech 1996;29:687–92. https://doi.org/10.1016/0021-9290(95)00125-5.
[25] Kottan N, Gowtham NH, Basu B. Development and validation of a finite element model of wear in UHMWPE liner using experimental data from hip simulator studies. J Biomech Eng 2022;144:031001. https://doi.org/10.1115/1.4052373.
[26] Mattei L, Di Puccio F, Ciulli E, Pauschitz A. Experimental investigation on wear map evolution of ceramic-on-UHMWPE hip prosthesis. Tribol Int 2020;143:106068. https://doi.org/10.1016/j.triboint.2019.106068.
[27] Ruggiero A, Sicilia A. A mixed elasto-hydrodynamic lubrication model for wear calculation in artificial hip joints. Lubricants 2020;8:72. https://doi.org/10.3390/lubricants8070072.
[28] Maxian TA, Brown TD, Pedersen DR, Callaghan JJ. Adaptiive finite element modeling of long-term polyethylene wear in total hip arthroplasty. J Orthop Res 1996;14:668–75.
[29] Matsoukas G, Kim IY. Design optimization of a total hip prosthesis for wear reduction. J Biomech Eng 2009;131:051003. https://doi.org/10.1115/1.3049862.
[30] Zeman J, Ranuša M, Vrbka M, Gallo J, Křupka I, Hartl M. UHMWPE acetabular cup creep deformation during the run-in phase of THA's life cycle. J Mech Behav Biomed Mater 2018;87:30–9. https://doi.org/10.1016/j.jmbbm.2018.07.015.
[31] Mattei L, Tomasi M, Artoni A, Ciulli E, Di Puccio F. Combination of musculoskeletal and wear models to investigate the effect of daily living activities on wear of hip prostheses. Proc Inst Mech Eng Part J J Eng Tribol 2021;235:2675–87. https://doi.org/10.1177/13506501211058239.
[32] Srivastava G, Christian N, Fred Higgs C. A predictive framework of the tribological impact of physical activities on metal-on-plastic hip implants. Biotribology 2021;25:100156. https://doi.org/10.1016/j.biotri.2020.100156.
[33] Ruggiero A, Sicilia A, Affatato S. In silico total hip replacement wear testing in the framework of ISO 14242-3 accounting for mixed elasto-hydrodynamic lubrication effects. Wear 2020;460–461:203420. https://doi.org/10.1016/j.wear.2020.203420.